Charmonium spectroscopy from inclusive ψ' and J/ψ radiative decays

J. E. Gaiser,[a] E. Bloom, F. Bulos, G. Godfrey, C. Kiesling,[b] W. Lockman,[c] M. Oreglia,[d] and D. L. Scharre[e]
Stanford Linear Accelerator Center, Stanford University, Stanford, California 94305

C. Edwards,[f] R. Partridge,[c] C. Peck, and F. C. Porter
Physics Department, California Institute of Technology, Pasadena, California 91125

D. Antreasyan, Y. F. Gu,[g] J. Irion, W. Kollman,[h] K. Strauch, K. Wacker,[i] and A. Weinstein[c]
Lyman Laboratory of Physics, Harvard University, Cambridge, Massachusetts 02138

D. Aschman,[j] T. Burnett,[k] M. Cavalli-Sforza,[c] D. Coyne,[c] C. Newman,[l] and H. F. W. Sadrozinski[c]
Physics Department, Princeton University, Princeton, New Jersey 08544

D. Gelphman,[m] R. Hofstadter, R. Horisberger,[n] I. Kirkbride, H. Kolanoski,[o] K. Königsmann,[p] R. Lee,[f] A. Liberman,[q] J. O'Reilly,[r] A. Osterheld, B. Pollock,[s] and J. Tompkins
Physics Department and High Energy Physics Laboratory, Stanford University, Stanford, California 94305
(Received 16 December 1985)

Results from a detailed study using the Crystal Ball detector at the SLAC e^+e^- storage ring SPEAR of the inclusive photon spectra from 1.8×10^6 ψ' and 2.2×10^6 J/ψ decays are presented. Radiative transitions from the ψ' to the $\chi_{2,1,0}$ states are observed with photon energies of $126.0\pm0.2\pm4$, $169.6\pm0.3\pm4$, and $258.4\pm0.4\pm4$ MeV and branching ratios $B(\psi'\to\gamma\chi_{2,1,0})=(8.0\pm0.5\pm0.7)\%$, $(9.0\pm0.5\pm0.7)\%$, and $(9.9\pm0.5\pm0.8)\%$, respectively. Values for the natural linewidths of the χ states are obtained: $\Gamma(\chi_{2,1,0})=0.8$–4.9, <3.8, and 13–21 MeV, respectively (90% C.L.). Improved values are found for the branching ratios $B(\psi'\to\gamma\eta_c)=(0.28\pm0.06)\%$ and $B(J/\psi\to\gamma\eta_c)=(1.27\pm0.36)\%$, and for the natural width $\Gamma(\eta_c)=11.5\pm4.5$ MeV.

I. SPECTROSCOPY OF THE ψ FAMILY

Since the discovery of the resonances of the $c\bar{c}$ charmonium family more than a decade ago, the ψ' and J/ψ have continued to stimulate considerable theoretical and experimental interest to explore the spectrum of states accessible via radiative photon decays. Potential models[1] and dispersion-relation models[2] have predicted the spectrum of states, radiative transition rates, and natural linewidths, in lowest-order quantum chromodynamics (QCD). Calculations of relativistic and higher-order QCD corrections[3] have also been made. Two early experiments measured the inclusive photon spectra in J/ψ and ψ' decays. Ten years ago the Mark I magnetic detector, sensitive to converted photons above 200 MeV, discovered the $\psi'\to\gamma\chi_0$ transition[4] at the SLAC e^+e^- colliding ring SPEAR. In a short run at SPEAR the SP-27 experiment[5] used a moderately segmented NaI(Tl) detector to obtain a highly structured photon spectrum in ψ' decays. The ψ' radiative decay branching ratios to each of the triplet $1\,^3P_{2,1,0}(\chi_J)$ states[6] were measured and found to be significantly below the naive potential model predictions. In a more recent work[7] at the CERN ISR and using a very different technique, the $\chi_{2,1}$ states have also been measured. Furthermore, a candidate for the $1\,^1S_0$ ground state, the $\eta_c(2980)$ was observed in the inclusive photon spectra from ψ' and J/ψ decays by the Crystal Ball experiment.[8] This state was confirmed in exclusive decays of the ψ' by the Mark II experiment[9] and has recently been well measured by the Mark III experiment[10] which also determined the spin and parity to be 0^{-+}. The Crystal Ball also reported existence of a $2\,^1S_0$ candidate,[11] the $\eta_c'(3590)$ seen in the ψ' inclusive photon spectrum. A candidate for the $^1P_1$ state has not been observed so far.[12]

In this paper we present final results of a detailed study of the radiative transitions from ψ' to the triplet χ_J states using the Crystal Ball detector. The states are identified by observing monochromatic photon lines in the inclusive photon spectra associated with hadronic decays of the resonance. New measurements for the radiative decays of J/ψ and ψ' to the $\eta_c(2984)$, based on about twice the data sample of Ref. 8, are also presented. The photon spectra are obtained from decays of 1.8×10^6 ψ' and 2.2×10^6 J/ψ, produced with integrated luminosities of 3450 and 770 nb^{-1}, respectively.

II. THE CRYSTAL BALL DETECTOR

The Crystal Ball detector is particularly suited to study the radiative transitions in the charmonium system. The main design goal was to provide a high resolution measurement of energy and direction of electromagnetically showering particles over a large solid angle. Figure 1 shows the schematic of the detector. Full details of the

 ©1986 The American Physical Society

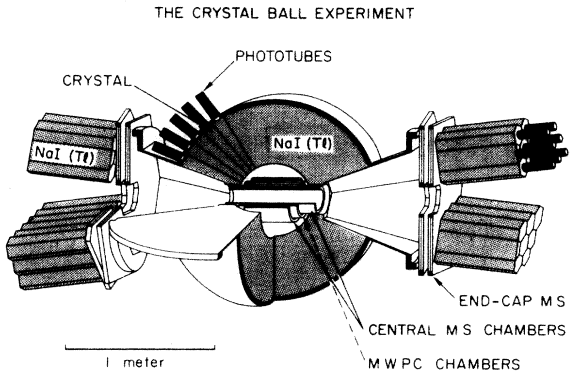

FIG. 1. Schematic view of the Crystal Ball detector.

detector have been reported elsewhere.[13–15] It consists of a spherical and highly segmented shell of 672 NaI(Tl) shower counters covering 93% of the 4π solid angle. Additional NaI(Tl) end-cap counters increase the coverage to 98% of 4π. The NaI(Tl) shell is 16 inches thick, corresponding to 16 radiation lengths (r.l.) and to one nuclear absorption length. The energy resolution for photons (see Sec. VII) is measured to be $\sigma(E)/E=(2.4–2.8)\%/E^{1/4}$, where E is the energy in GeV. The angular resolution is slightly energy dependent, varying between 30 and 50 mrad. Charged particles are identified by a concentric system of two cylindrical magnetostrictive wire spark chambers sandwiching a multiwire proportional chamber. The chambers cover 0.71, 0.83, and 0.94 of the 4π solid angle. Neutral tracks are identified by the electromagnetic shower in the NaI(Tl) crystals and the lack of signals in the central spark and proportional chambers.

The apparatus was triggered when at least one of several overlapping conditions was satisfied. The primary and dominant trigger requires the total energy deposited in the Crystal Ball (excluding the end caps) to be greater than $\simeq$1.1 GeV. Other triggers, which are somewhat redundant, are based on charged-particle multiplicities being detected by the chambers or on the general energy distribution pattern in the Ball. Studies of Monte Carlo–simulated events show the trigger efficiency to be $\simeq$99% for inclusive hadronic decays of ψ' and J/ψ.

The photon energy scale is set by measuring large-angle Bhabha scattering events ($e^+e^-\rightarrow e^+e^-$ and $\gamma\gamma$) as well as direct e^+e^- decays of J/ψ and ψ'. A calibration of the NaI(Tl) crystals and associated electronics was performed every two weeks during data taking. The calibration used the above reactions in conjunction with radioactive γ-ray sources and γ rays from the proton induced reaction $^{19}\mathrm{F}(p,\alpha)^{16}\mathrm{O}^*$ using a Van de Graaff accelerator. The use of a linear relation for the energy calibration results in a small, $\simeq$(2–3)%, energy shift towards lower photon energies as determined from observed mass values of reconstructed π^0 and η particles. It is an indication of our systematic uncertainty in the energy scale.

The Crystal Ball with its unique geometrical segmentation provides not only a measurement of the amount of energy deposited but also gives information about the transverse structure of this deposit. Photons (and electrons) with energies of greater than about 20 MeV produce electromagnetic showers and deposit almost all their energy into the 13 neighboring crystals around the impact point. These electromagnetic showers display very regular transverse shower development, causing symmetric lateral energy distribution patterns. Their fluctuations are relatively small, though occasional large fluctuations do occur. In contrast, interacting charged hadrons produce extremely varied energy patterns in the NaI(Tl). Their fluctuations are large and irregular when compared to electromagnetic showers. A still different response of the detector is found for noninteracting minimum ionizing particles. They deposit an energy of about 210 MeV distributed in no more than two or three crystals. Lastly there are ambiguous energy patterns resulting from the merging of photon showers with energy deposits from hadronic interactions.

The detector provides no information about the longitudinal distribution of an energy deposition. It has been found that a detailed analysis of the lateral energy distribution patterns is a very useful technique for resolving photon identification ambiguities. Examples of typical lateral energy distribution patterns for charged particles and photons are shown in Fig. 2; the figure represents the data

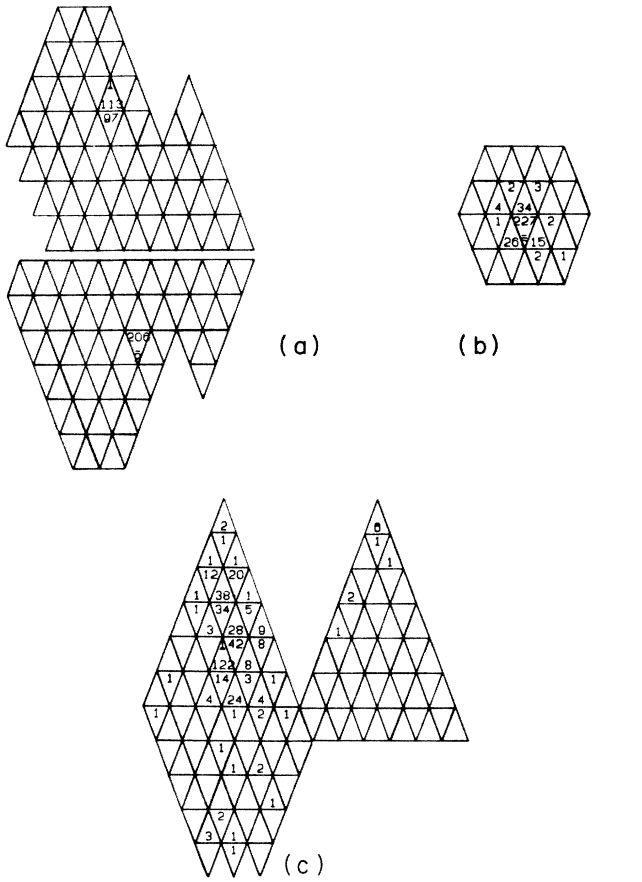

FIG. 2. Typical lateral energy distribution patterns in the NaI(Tl). Numbers represent energy (in MeV) deposited in individual crystals. (a) Example of crystal energy distributions for two minimum ionizing particles. (b) Example of an energy distribution for an electromagnetically showering particle. (c) Example of an energy distribution for an interacting charged hadron.

as Mercator projections of segments of the detector. Algorithms have been developed which can distinguish clean photons from charged particles based on their energy patterns, like those shown in Fig. 2. Identification of photons with these algorithms plays an important part in this spectroscopic analysis.

III. DATA SELECTION

The selection of radiative ψ' and J/ψ decays is done in two steps. First, hadronic decays of the resonances are selected. Second, the photons in these events are identified. In this section we describe how these selections are carried out.

A. Hadronic-event selection

The e^+e^- annihilation events leading to multihadron final states must be separated from backgrounds due to cosmic rays traversing the detector, beam-gas interactions, and showering quantum-electrodynamics (QED) events from the processes $e^+e^- \rightarrow e^+e^-(\gamma)$ and $e^+e^- \rightarrow \gamma\gamma(\gamma)$. The beam-gas events and cosmic-ray events typically deposit small amounts of energy in the ball, or else deposit energy in a highly asymmetric pattern. Showering QED events deposit almost the entire e^+e^- center-of-mass energy in two or three showers. Total energy and energy distribution criteria are used to remove these sources of background. The efficiency of the hadronic-event-selection procedure is estimated by Monte Carlo simulation of hadronic events to be 0.94 ± 0.05. Full details on the selection criteria and efficiency determination are given in Ref. 15. Using triggers out of time with the beam crossings, separated beam runs, and Monte Carlo simulation of showering QED events, it is estimated that the contamination of the selected hadronic sample by cosmic rays, beam-gas events, and QED events is only 0.010 ± 0.005. Since the J/ψ and ψ' resonance production cross sections are very large, only $\simeq 1\%$ of the events in the J/ψ sample, and $\simeq 3\%$ in the ψ' sample are nonresonant. For the same reason, the number of e^+e^- interactions proceeding via the two-photon process is small, and nearly all of these are removed by the total energy and energy symmetry requirements for hadronic events. The net effect of all cuts results in a clean sample of J/ψ and ψ' hadronic decays.

To arrive at the final number of produced resonances $N_{\rm prod}$, small corrections are made for residual contaminations due to cosmic rays, beam-gas interactions, showering QED events, nonresonance background, resonance decays to lepton pairs, and the hadron-selection efficiency (0.94 ± 0.05).

B. Photon selection

Energy spectra of all photon candidates produced in hadronic decays of the ψ' and J/ψ contain monochromatic photon lines on top of a large background. The background results from several sources are the following.

(1) Photons, predominantly from decays of π^0 and η mesons, which are produced in multihadronic decays. These photons will have a smooth distribution, similar to that in nonresonant e^+e^- annihilation.

(2) Photons from the decay of monoenergetic η mesons produced in the two-body decay $\psi' \rightarrow \eta J/\psi$, which produce a nonsmooth distribution.

(3) Energy deposited by charged particles which have escaped detection by the tracking chambers and are then misidentified as neutrals.

(4) Remnants from nuclear interactions of charged hadrons in the NaI(Tl) causing additional energy deposits which are well separated from the original impact point. Such neutral-energy "split offs" (usually near 50 MeV) will fake a photon.

With the advantage of a large data set, stringent as well as loose photon-selection criteria can be employed to suppress background while retaining a significant signal. By using widely different cuts, it is possible to perform a parametric study to examine the effect of the cutting process on energies, branching ratios, and natural line widths. Also, we are able to assess the magnitude of systematic errors attributable to the background under the photon peaks and to our estimate of the photon detection efficiency. The following cumulative selection criteria are applied to the data to yield the four ψ' inclusive photon spectra shown in Fig. 3.

(a) Removal of neutrals and charged tracks with $|\cos\theta| > 0.85$, where θ is the angle between the track and the positron beam direction. The solid-angle restriction ensures that the particle has entered a region in the detector with uniform acceptance, away from the edges, to give optimum energy resolution. Since both neutral and charged tracks are present in this spectrum a very large

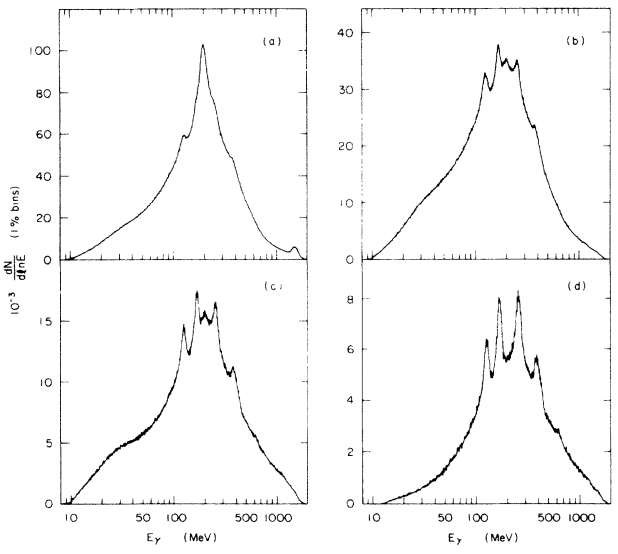

FIG. 3. Inclusive photon spectra from ψ' decays in 1% energy bins. (a) All tracks within $|\cos\theta| < 0.85$. (b) Same as (a) with charged tracks removed. (c) Same as (b) with neutrals from π^0 decays and neutral particles near interacting charged particles removed. (d) Same as (c) with neutral particles removed, whose lateral energy deposition is not consistent with the pattern of a typical single electromagnetic showering particle.

peak at $\simeq$210 MeV is observed, corresponding to noninteracting charged particles passing through the detector. This peak constitutes a considerable background which greatly obscures the χ_J lines. Nevertheless the signals are significant and can be measured.

(b) Removal of charged tracks using information from the tracking chambers. This cut removes most of the charged particles as can be seen by the strong reduction in relative size of the minimum ionizing structure at $\simeq$210 MeV. The persistance of a small remnant bump at this energy is indicative of a certain inefficiency in the charged-particle identification.

(c) Removal of neutral pairs which can be fitted to $\pi^0 \rightarrow \gamma\gamma$ decays using the entire acceptance of the detector to reduce the number of background photons in the spectrum. We also remove neutral particles too close to interacting charged particles, $\cos\theta_{i,j} > 0.85$ (where $\theta_{i,j}$ is the angle between the pair of tracks). This cut minimizes distortions of the photon energy.

(d) Removal of neutral particles, whose lateral shower deposition patterns in the NaI(Tl) do not conform to those of single clean electromagnetic showers, as identified by our photon recognition algorithms. This cut removes virtually all remaining minimum ionizing and interacting charged particles which were not detected in (b) because of inefficiencies in the charged tracking. It also eliminates the asymmetric energy depositions from split offs, visible as the broad bump near 50 MeV in Fig. 3(c).

IV. THE ψ' INCLUSIVE PHOTON SPECTRUM

A comparison of the spectra in Figs. 3(a)—3(d) shows a dramatic enhancement of signal to noise as the cuts are applied. Prominent features in the spectra include three lines due to the monochromatic photons from the decays $\psi' \rightarrow \gamma\chi_{2,1,0}$ at $\simeq$126, 170, and 258 MeV, respectively.

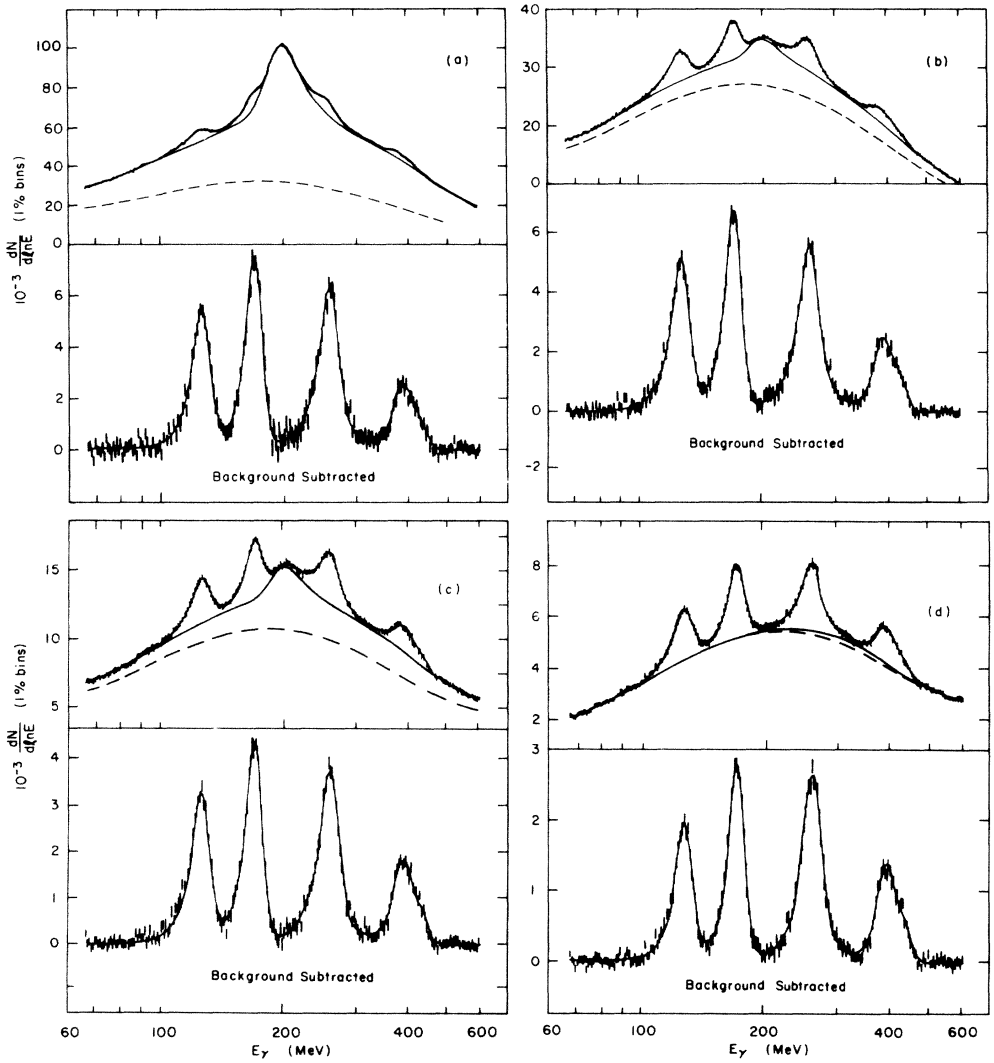

FIG. 4. Fits to the inclusive photon spectra of Fig. 3 using the techniques described in the text. The dashed curve in the upper part of each figure represents the smooth photon background as modeled by the Legendre-polynomial series. The solid curve represents the background due to charged particles and the decay ($\psi' \rightarrow \eta J/\psi$). The bottom portion of each figure shows the result of subtracting the fitted background.

Also prominent is a signal near 400 MeV from the two overlapping and Doppler-broadened lines corresponding to the secondary transitions $\chi_{2,1}\to\gamma J/\psi$ at 432 and 392 MeV, where the χ particle recoils against the primary photon. Because of the finite detector resolution, the two lines overlap. A small peak is seen in the fully cut spectrum [Fig. 3(d)] near 634 MeV, corresponding to the transition $\psi'\to\gamma\eta_c(2984)$. Because of the fine binning (1%) used in this spectrum, the signal near 92 MeV due to the transition $\psi'\to\gamma\eta_c'(3592)$ is not readily apparent.[11]

By looking at Fig. 3, it becomes obvious that the crowded and overlapping signals on top of the broad and peaked background cannot be measured by fitting only a local portion of the spectra. In order to reliably measure the χ_J signal amplitudes, the peak photon energies and the natural linewidths of the states, it is necessary to have a detailed model which adequately describes signal behavior and background distributions over the whole range of interest. Fits to the four spectra are performed in the range of 65 MeV $<E_\gamma<600$ MeV, excluding the energy region of the η_c (the analysis of the η_c signal region is described in Sec. VI), using a model which consists of the sum of the following individual contributions.

(1) To describe the signals, the detector's intrinsic energy response function is parametrized using a Gaussian distribution with a power-law tail to low energies, starting at $\simeq 1\sigma$ below the peak and joined to the Gaussian with continuous first derivative. This response function is convoluted with a nonrelativistic Breit-Wigner mass distribution for the widths of the χ states. Together the two sources yield the total signal widths. The transition matrix elements for the χ_J transitions are taken to be dominantly electric dipole,[14] leading to an $E_\gamma{}^3$ energy dependence in the folded signal shape. Positions of the peaks, amplitudes, widths, and response function parameters are allowed to vary in the fit. For the secondary transitions $\chi_{2,1}\to\gamma J/\psi$ the expected Doppler broadening is also taken into account in the fit. The secondary photon energies are fixed by the energies of the primary line and the masses of the ψ' and J/ψ. No signal corresponding to the decay $\chi_0\to\gamma J/\psi$ is visible in the inclusive photon spectrum.

(2) To describe the background under the photon peaks three sources are included in the fit. (i) A Legendre polynomial series of fourth order [fifth order for spectrum 2(d)] describes the smooth photon background. (ii) A charged-particle spectrum is used with variable amplitude and fixed shape to take into account the charged-particle contribution. The shape of the spectrum is obtained by taking genuine charged particles defined by the tracking chambers which also satisfy the photon selection cuts. (iii) A fixed amplitude is used for the contribution from the decay $\psi'\to\eta J/\psi\to\gamma\gamma J/\psi$, based on the measured branching ratio.[14] Its shape is derived from a Monte Carlo simulation of the decays $\eta\to\gamma\gamma$, whose photons are added to real J/ψ events. The contribution from decays $\psi'\to\pi^0\pi^0 J/\psi$ is found to have a negligible effect on the fitted signal amplitudes and natural line widths and is not included in the fit.

The resulting fits to the four spectra are shown in Fig. 4. The χ^2 confidence levels of the fits range from 12% to 52%, indicating that the model describes signal shapes and backgrounds consistent with the data. The energies of the photon lines, obtained by a weighted average of the peak positions from all fits for $\chi_{2,1,0}$, are $126.0\pm0.2\pm4$, $169.6\pm0.3\pm4$, and $258.4\pm0.4\pm4$ MeV, respectively. The first error is statistical, due to the uncertainty of the photon energy determination by the fit. The second error, which is systematic, is mainly due to the uncertainty in the energy scale.

V. TRANSITIONS TO THE χ_J STATES IN ψ' RADIATIVE DECAYS

The branching ratios for the observed transitions are calculated according to

$$B=\frac{(N_\gamma/\epsilon_\gamma)}{N_{\rm prod}\epsilon_{\rm fs}}\ , \tag{1}$$

where N_γ is the fitted number of photons in a given peak, $N_{\rm prod}$ is the number of ψ' resonances produced, and ϵ_γ is the overall detection efficiency for photons of given energy E_γ. Included in this efficiency is the photon selection efficiency calculated as described below, losses due to conversion of photons in the beam pipe and the chambers (0.035 ± 0.005), and a geometric correction factor for the photon angular distributions ($1+\cos^2\theta$ for the χ_0, $1-0.189\cos^2\theta$ for the χ_1, and $1-0.052\cos^2\theta$ for the χ_2, see Ref. 14). The efficiency to detect the final state $\epsilon_{\rm fs}$ is 0.94 ± 0.02, where the normalization error common to $N_{\rm prod}$ has been removed.

Estimates of the photon selection efficiency are made using Monte Carlo techniques at five energies ($E_\gamma=90$, 145, 210, 320, and 500 MeV) spanning the range of the observed peaks for each of the spectra shown in Fig. 3. At each energy a large sample of 5×10^4 monochromatic photons is generated isotopically. The distribution of electromagnetic shower energy in the crystals is calculated using the EGS electromagnetic shower code.[16] Each Monte Carlo photon is added to a real J/ψ event from the data sample, to produce a hybrid event simulating the decay[17] $\psi'\to\gamma\chi$. Here we assume that multihadronic χ decays resemble multihadronic J/ψ decays sufficiently closely for the purposes of calculating photon detection efficiencies. These events are then processed with the same analysis algorithms and photon selection cuts described above. Finally the Monte Carlo spectrum is added to the appropriate ψ' spectrum to give it a realistic background. The resulting spectrum, now containing an additional photon line besides the already existing χ lines, is fitted using the technique of Sec. IV. The photon selection efficiency is calculated by comparing the fitted Monte Carlo signal to the number generated and is shown in Fig. 5. Studies of the variation in efficiency, with respect to background and signal size and photon-selection cuts, give an estimated point to point error in efficiency of about $\pm4\%$ and an absolute error of $\pm5\%$.

For each decay $\psi'\to\gamma\chi_J$ and $\chi_J\to\gamma J/\psi$ four evaluations of the branching ratio corresponding to the four spectra of Fig. 3 are made. By comparing the branching ratios $B(\psi'\to\gamma\chi_J)$ from each of the four spectra, one is able to qualitatively check the estimate in the magnitude

of the systematic errors due to the fitting procedure. The results are summarized in Fig. 6. The errors shown are due to statistical uncertainties in the fits only. As can be seen, by reading across the figure, the branching ratios obtained from the differently selected spectra are reasonably consistent. Considering the wide variation in background shapes and efficiencies, the fact that consistent results are obtained gives confidence to the procedure of extracting the branching ratios.

Another check is performed by comparing the cascade branching ratio $B(\psi'\to\gamma\chi_{2,1})B(\chi_{2,1}\to\gamma J/\psi)$, from the secondary transition lines at about 400 MeV from the inclusive spectra, with the values obtained from an analysis of the exclusive cascade reaction $\psi'\to\gamma\gamma J/\psi\to\gamma\gamma$ (e^+e^- or $\mu^+\mu^-$) using the Crystal Ball detector.[14] The results of the exclusive cascade measurements are displayed on the bottom of Fig. 6 as the dashed bands. The inclusive measurements of the product branching ratio for the χ_2 (shown as the data points) are consistently lower than the exclusive measurements, whereas the values for the χ_1 tend to be somewhat higher. When taking the sum of the two branching ratios, good agreement between inclusive and exclusive analyses is reached. This systematic effect is due to the overlap of the two lines in the inclusive spectra where the relative strengths of the signals can only be poorly determined by the fit.

The branching ratios of the χ_J analysis are given in Table I. The values shown for the $B(\psi'\to\gamma\chi_J)$ and the product branching ratios $B^2(\chi_J)\equiv B(\psi'\to\gamma\chi_J)B(\chi_J\to\gamma J/\psi)$, are derived by averaging the four branching ratios, weighted by their errors (a combination of the statistical error from the fit and the statistical error in the photon detection efficiency). The effect of the weighting process is to slightly de-emphasize the results from the uncut spectrum containing charged and neutral particles. Combining the values by averaging is based on the assumption that the measurement errors among the spectra are largely independent, since they are driven by the fitting process where the spectra have very different background shapes and signal strengths. Two errors are given for each branching ratio. The first error contains the statistical uncertainty from the fit plus the point-to-point statistical

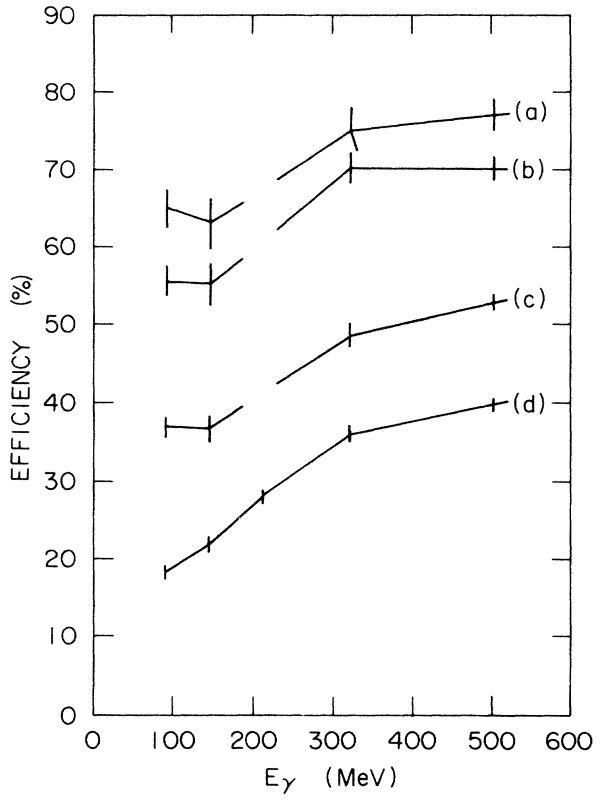

FIG. 5. Photon-selection efficiencies as a function of energy for the different selection criteria. The letters correspond to the photon-selection criteria used to obtain the spectra of Fig. 3. These values assume a flat photon angular distribution and do not account for photon conversion in the inner detector. The error bars are from fits to the Monte Carlo lines described in the text. The region around 210 MeV is complicated by the significant punch through from minimum-ionizing particles for the photon selection criteria (a)–(c) only and is thus not calculated.

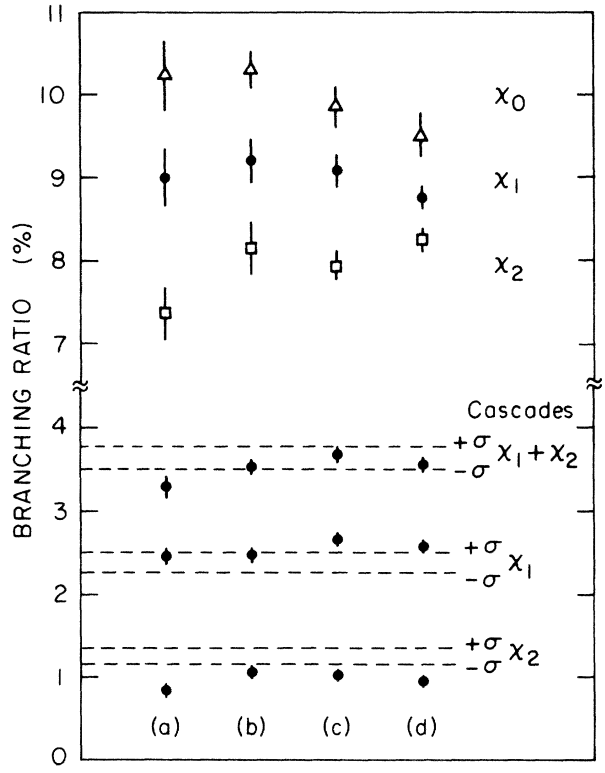

FIG. 6. The upper part of the figure shows the observed branching ratios $B(\psi'\to\gamma\chi_{2,1,0})$ as obtained from independent analyses of each of the spectra of Fig. 3. This serves as a crosscheck on the extraction of the branching ratios. In the lower part of the figure are the product branching ratios $B(\psi'\to\gamma\chi_{2,1})B(\chi_{2,1}\to\gamma J/\psi)$ obtained from the four inclusive spectra (dots). Only statistical errors are shown. They are compared with the results of the direct measurement of the cascade $\psi'\to\gamma\gamma l^+l^-$ (dashed bands) by the Crystal Ball (Ref. 14). Since the separation of the overlapping lines from the secondary transitions $\chi_2\to\gamma J/\psi$ and $\chi_1\to\gamma J/\psi$ in the inclusive spectra is difficult, the comparison with the sum of the branching ratios is also shown.

TABLE I. Results for the transitions $\psi' \to \gamma\chi_J$. The photon energies and rates for $\psi' \to \gamma\chi_{2,1,0}$ obtained from the fitted inclusive photon spectra in decays of the ψ' are presented here. Also listed are the product branching ratios $B^2(\chi_J) \equiv B(\psi' \to \gamma\chi_J)B(\chi_J \to \gamma J/\psi)$, the branching ratios $B(\chi_J \to \gamma J/\psi)$ and the widths of the χ_J states. The correlation coefficient between the $B^2(\chi_2)$ and the $B^2(\chi_1)$ measurements is about 0.2 (see Sec. V).

Quantity	χ_2	χ_1	χ_0
E_γ (MeV)	126.0±0.2±4	169.6±0.3±4	258.4±0.4±4
$B(\psi' \to \gamma\chi_J)$ (%)	8.0±0.5±0.7	9.0±0.5±0.7	9.9±0.5±0.8
$B^2(\chi_J)$ (%)	0.99±0.10±0.08	2.56±0.12±0.20	Not seen here
$B(\chi_J \to \gamma J/\psi)$ (%)	12.4±1.5	28.4±2.1	See text
Γ (MeV) 90% C.L.	0.8–4.9	<3.8	13–21

uncertainty in the photon detection efficiency. The second error contains all the uncertainty in the overall normalization and is mainly due to the systematic error in the number of resonances produced (±5%) and to an absolute uncertainty in the photon detection efficiency (±5%). The error attributable to the systematic uncertainty in the detector's energy resolution is only $\simeq \pm 1\%$.

Dividing the product branching ratios $B^2(\chi_{2,1})$ by the results for $B(\psi' \to \gamma\chi_{2,1})$, yields the branching ratio $B(\chi_{2,1} \to \gamma J/\psi)$. Note that in these calculations the normalization errors cancel. To obtain our best measurement for the branching ratio $B(\chi_0 \to \gamma J/\psi)$ (this transition is not seen in the inclusive analysis) we use the Crystal Ball exclusive channel product branching ratio,[14] $B^2(\chi_0) = (0.059 \pm 0.017)\%$, and divide it by the inclusive result for $\psi' \to \gamma\chi_0$. In this case only the common normalization error due to the uncertainty in the number of ψ' resonances produced cancels. We obtain $B(\chi_0 \to \gamma J/\psi) = (0.60 \pm 0.18)\%$.

VI. TRANSITIONS TO THE η_c IN ψ' AND J/ψ RADIATIVE DECAYS

Additional data obtained since an earlier Crystal Ball study[8] of the transitions $\psi' \to \gamma\eta_c$ and $J/\psi \to \gamma\eta_c$ in the inclusive photon spectra permit an analysis based on 1.8×10^6 ψ' and 2.2×10^6 J/ψ events, which is about twice the number of events available previously. The procedure to extract the signals is quite similar to the one described in the above section for the $\psi' \to \gamma\chi_J$ transitions except that the photon lines are sufficiently isolated so that a local fit can be used to measure the signal. The decay $\psi' \to \gamma\eta_c$ is assumed to be a hindered magnetic dipole transition.[18] To account for this a factor of E_γ^7 is included in the convolution of the detector's response function with the η_c Breit-Wigner resonance shape for this transition. For the allowed magnetic dipole transition $J/\psi \to \gamma\eta_c$ the usual factor E_γ^3 is used. Three photon-selection criteria, for both ψ' and J/ψ, are applied to esti-

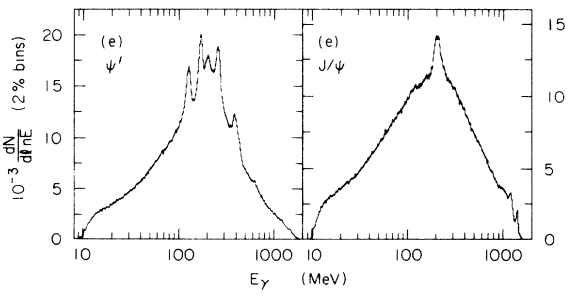

FIG. 7. Inclusive photon spectra from ψ' and J/ψ decays in 2% energy bins, obtained with the modified cut (e) on the lateral energy distribution as described in the text. This cut has less rejection power against charged particles than cut (d) as can be seen by the structure at ≃210 MeV, due to minimum ionizing particles.

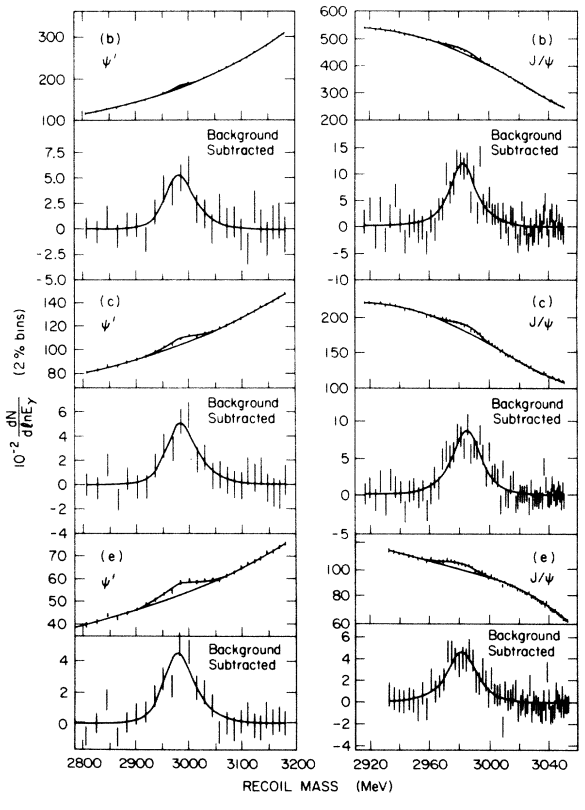

FIG. 8. Simultaneous fits to the η_c mass in the ψ' and J/ψ inclusive photon spectra. The data are plotted in 2% bins in the photon energy. The preferred resolution value of $\sigma_0 = 2.7\%$ is used in the fit. The spectra labeled (b) and (c) correspond to the photon selection criteria of the χ analysis. The spectra labeled (e) employ a modified cut on the lateral photon energy pattern as described in the text.

mate the sensitivity of results to cuts and background shapes. Two spectra from the ψ' [Figs. 3(b) and 3(c)] together with corresponding spectra from the J/ψ (not shown) are studied. In addition, a third spectrum (e) is produced for both ψ' and J/ψ which incorporates a looser cut on the lateral shower deposition pattern [cut (d) of the ψ' analysis] and is shown in Fig. 7. This cut optimizes the detection efficiency for low-energy photons but, at the same time, reduces the rejection of charged particles as compared to cut (d). For each set of cuts a simultaneous fit is made to the ψ' and J/ψ inclusive photon spectra with the η_c mass and width constrained to be the same for both spectra in the pair. Figure 8 shows the fits to the three pairs of ψ' and J/ψ spectra.

The mass of the η_c is obtained by averaging the results from the three fits and is given in Table II. The first error is statistical. The second error is systematic and mainly due to the uncertainty in the absolute energy scale.

The branching ratios are calculated using Eq. (1) in Sec. V. The efficiency to detect the final state for the radiative J/ψ transition is 0.94 ± 0.02 and 0.96 ± 0.02 for the radiative ψ' transition, where the normalization error common to $N_{\rm prod}$ has been removed. The photon detection efficiencies for the transition $\psi'\to\gamma\eta_c$ with $E_\gamma\simeq634$ MeV are determined to be $(62\pm5)\%$, $(50\pm5)\%$, and $(46\pm5)\%$ for the spectra (b), (c), and (e), respectively. For the transition $J/\psi\to\gamma\eta_c$ at $E_\gamma\simeq108$ MeV they are found to be

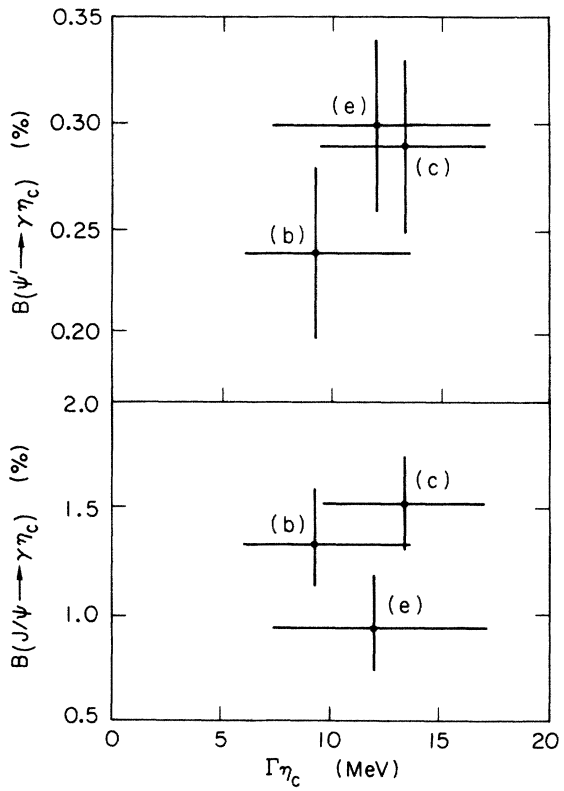

FIG. 9. Comparison of the fitted η_c natural linewidth and branching ratios from ψ' and J/ψ, obtained from the three simultaneous fits in Fig. 8. The errors include contributions from the statistical uncertainty in the fit and from the uncertainty in the detector's resolution.

TABLE II. Results for the transitions $\psi'\to\gamma\eta_c$ and $J/\psi\to\gamma\eta_c$. The mass of the η_c and the branching ratios for the transitions $\psi'\to\gamma\eta_c$ and $J/\psi\to\gamma\eta_c$, obtained from the fitted inclusive photon spectra of the ψ' and J/ψ, are presented. Also listed is the width of the η_c.

Quantity	η_c
Mass (MeV)	$2984.0\pm2.3\pm4.0$
$B(\psi'\to\gamma\eta_c)$ (%)	0.28 ± 0.06
$B(J/\psi\to\gamma\eta_c)$ (%)	1.27 ± 0.36
Γ (MeV)	11.5 ± 4.5

$(50\pm5)\%$, $(32\pm5)\%$, and $(24\pm5)\%$ for the spectra (b), (c), and (e), respectively. A common geometric factor for the photon angular distribution of $1+\cos^2\theta$ is used for all spectra.[10] Table II summarizes the pseudoscalar branching ratios obtained by averaging the results from each spectrum. The error due to the small signal size dominates all other uncertainties. Therefore all contributions to the uncertainty are combined into one single error.

Figure 9 gives a two-dimensional comparison of the η_c width (discussed in Sec. VII) and branching ratios, $B(\psi'\to\gamma\eta_c)$ and $B(J/\psi\to\gamma\eta_c)$, obtained from the three fitted spectra. Only statistical errors in the branching ratios from the fit are shown. The error on the width is a combination of statistical uncertainty from the fit and systematic uncertainty in the detector resolution. The three determinations are in reasonable agreement.

VII. THE NATURAL LINEWIDTHS

A. Width analysis

The analysis of the observed signals in the fitted inclusive photon spectra allows for the possibility of measuring the product state's natural linewidths.[19] Practically speaking, the quality of the natural line-shape measurement depends on two interrelated factors: (i) the statistical significance of the observed signal width $\Gamma_{\rm sig}$, and (ii) the relative size of the state's width Γ compared to the detector's resolution $\Gamma_{\rm res}$. The uncertainty in the Γ measurement results from a complicated relation between how precisely $\Gamma_{\rm sig}$ is known (which depends on the measured width's statistical significance), how precisely $\Gamma_{\rm res}$ is known (which depends on how well the detector is understood), and how large $\Gamma_{\rm sig}$ is compared to $\Gamma_{\rm res}$. Although the fitted signal amplitudes are found to be fairly insensitive to variations in the resolution, the fitted natural linewidths vary inversely with the resolution, and for the more narrow states ($\chi_{1,2}$), in a nonlinear way. The widths of the narrow states are very sensitive to small changes in the resolution.

The Crystal Ball detector's photon energy resolution used in this study is given by $\sigma(E)/E=\sigma_0/E^\alpha$, where the range of values in the resolution parameter σ_0 is (2.4–2.8)% (90% C.L.) and E is in GeV. This range includes an uncertainty in the exponent of the photon energy $\alpha=(0.25-0.30)$. The limits on σ_0 are obtained by fitting each ψ' inclusive photon spectrum in Fig. 3 at various fixed values of σ_0 as described in Sec. IV. All other pa-

rameters are allowed to vary and the variation in the χ^2 significance of the fit is examined. The upper and lower values in the resolution are those σ_0 values which yield a variation in χ^2 of 2.7 on either side of the minimum. The results differ slightly from spectrum to spectrum with the greatest deviation observed in the uncut spectrum Fig. 3(a). To obtain the final limit (2.4–2.8)% the lowest limit and the highest limit of the four spectra are used.

The upper limit on σ_0 is dominated by the fitted natural linewidth of the narrowest state: $\chi_1(3510)$.[20] Its fitted width rapidly approaches zero as σ_0 increases. This result sets an upper limit on the resolution for a photon energy of 170 MeV, but does not directly give information on the resolution at 126 or 260 MeV (corresponding to the transitions $\psi' \to \gamma\chi_{2,0}$, respectively). Considering the lower limit on σ_0, it is expected that the observed photon resolution in inclusive spectra will be worse than in clean low-multiplicity exclusive channels. It has been verified by Monte Carlo studies that the photon energy resolution is degraded in the environment of hadronic decays characterized by high-multiplicity events with subsequent hadron interactions in the NaI(Tl). Therefore the lower limit $\sigma_0 = 2.4\%$ is reasonable when compared with the Crystal Ball study of the exclusive cascade reaction[14] $\psi' \to \gamma\gamma J/\psi \to \gamma\gamma$ (e^+e^- or $\mu^+\mu^-$), involving the same photon transitions, where a resolution of $\sigma_0 = 2.6\%$ is found.

B. $\psi' \to \gamma\chi_J$

The natural linewidths of the χ_J states are measured from each spectrum in Fig. 3 to check the influence of the photon-selection process and its interplay with the background shape on the measured widths. Table I summarizes the width measurements of the χ_J states obtained from the fits shown in Fig. 4. The error in the χ_J widths is dominated by the uncertainty in the intrinsic resolution, although relatively less so for the χ_0 width. The error ranges on this quantity reflect the statistical uncertainty from the fit combined with the systematic uncertainty in resolution and are expressed as 90%-confidence-level intervals. Figure 10 shows the variation of the fitted natural linewidths as a function of the intrinsic resolution σ_0. The error bars indicate the magnitude of the statistical error from the fit.

For the χ_0 transition, the observed signal width [full width at half maximum (FWHM) $\simeq$39 MeV] is substantially broader than the resolution (FWHM $\simeq$23 MeV) and results in a value for the χ_0's natural linewidth of 13–21 MeV. This is large compared to its uncertainty. The χ_0 natural linewidth has also been measured with the Crystal Ball by studying the exclusive reaction[21] $\psi' \to \gamma\chi_0 \to \gamma\pi^0\pi^0 \to 5\gamma$, with data from the same experiment as reported here. The observed signal width (FWHM $\simeq$30 MeV) reported by that study of the exclusive reaction is narrower than that obtained by the inclusive measurement. With a detector energy resolution in the same range as in the inclusive analysis, a lower value for the χ_0 natural linewidth of $\Gamma(\chi_0) = 8.8 \pm 1.3 \pm 1.5$ MeV is found. The two measurements agree within 2.2 standard deviations. Combining these two measurements the Crystal Ball detector's best estimate[22] of the natural linewidth of the χ_0 is $13.5 \pm 3.3 \pm 4.2$ MeV.

The measured width for the χ_1 (<3.8 MeV, 90% C.L.) is consistent with zero. The measured width for the χ_2 (0.8–4.9 MeV, 90% C.L.) has large errors relative to its width. An experiment[7] at the CERN ISR has made a more precise determination of the natural linewidth for the χ_2 and the χ_1 formed in the reaction $p\bar{p} \to \chi_{2,1} \to \gamma J/\psi \to \gamma e^+e^-$. They find $\Gamma(\chi_2) = 2.7^{+1.4}_{-0.9}$ MeV and $\Gamma(\chi_1) < 1.25$ MeV (90% C.L.), in good agreement with the measurements reported here.

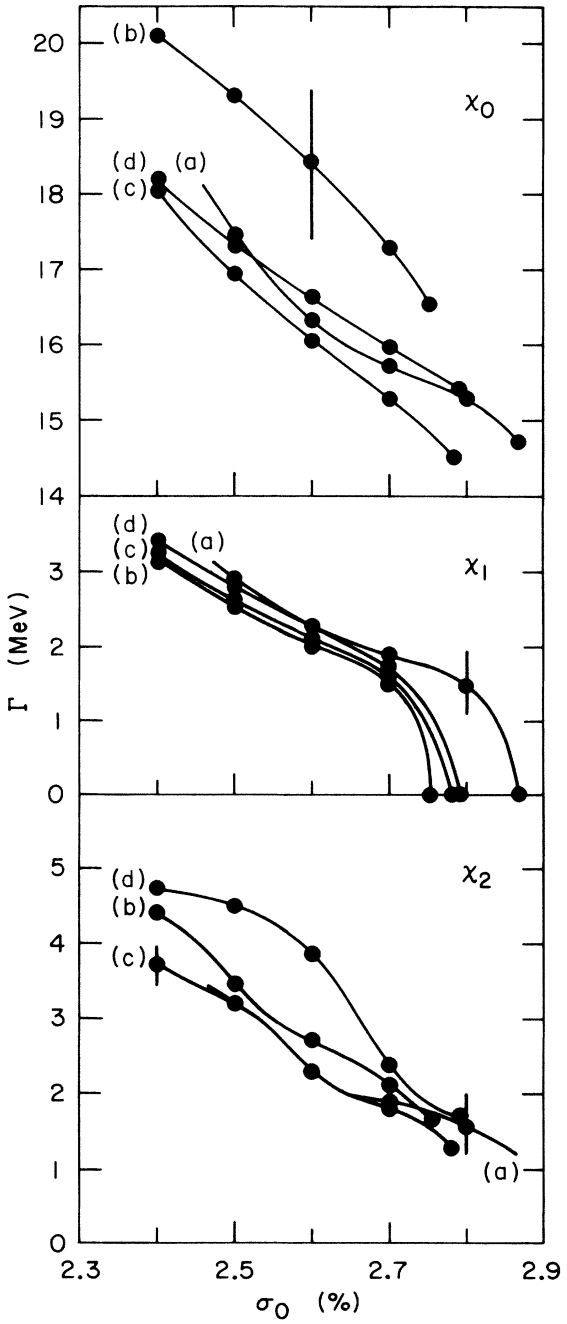

FIG. 10. Variation in the χ_J natural linewidth vs the photon intrinsic resolution for fits to the ψ' spectra shown in Figs. 3 and 4. The error bars indicate the statistical errors from the fit.

C. $\psi' \to \gamma\eta_c$ and $J/\psi \to \gamma\eta_c$

A similar analysis is used for the determination of the η_c width. The fits are shown in Fig. 8 and the results are tabulated in Table II. The η_c width measurement results almost entirely from the $J/\psi \to \gamma\eta_c$ signal where the detector's intrinsic full width resolution for photons of $\simeq 108$ MeV is $\Gamma_{\rm res} = 12 \pm 1$ MeV. This resolution is to be compared with that from the transition $\psi' \to \gamma\eta_c$ where the full width resolution for photons of $\simeq 634$ MeV is $\Gamma_{\rm res} = 45 \pm 7$ MeV. The purely statistical uncertainty in the fitted η_c natural linewidth from the combined simultaneous fit is ± 4.5 MeV. Consequently, the η_c natural linewidth measurement is primarily based on the signal from the $J/\psi \to \gamma\eta_c$ transition; the statistical error dominates the determination of the width.

VIII. CONCLUSIONS

With the measurements of the transitions from the ψ' to the χ states and to the η_c, presented in this paper, and the evidence for the η_c' state,[11] the Crystal Ball has measured nearly the whole spectrum of $c\bar{c}$ resonances, below the ψ' in inclusive radiative decays. Only the $^1P_1$ state has escaped experimental observation so far. This state is believed to be very difficult to detect in inclusive photon studies. The experiments measuring the charmonium states are in agreement with each other, concerning masses, branching ratios and the widths of the states.

Calculations to lowest-order QCD cannot be expected to correctly yield all the details of the system. For example, they predict the radiative transition branching ratios[23] well below the measured values (a factor of $\simeq 2$–3) and widths for the states[24] that are too small by about an order of magnitude.

Although the spacing of the states in the $c\bar{c}$ system is small when compared to the quark masses, suggesting a rather nonrelativistic system, it is known that relativistic effects do play a significant role. In addition, it is important to remember that the models used cannot be calculated directly from QCD first principles, but serve as a phenomenological description of the expected behavior of the potentials. This is the motivation to include known and calculable higher-order corrections inspired by QCD.

Incorporating these modifications, some models are indeed fairly successful in describing the spectrum of the states and the radiative branching ratios of the states.[25] On the other hand, it is also true that no calculation (so far) predicts correctly the totality of all the measurements.

ACKNOWLEDGMENTS

We gratefully acknowledge the efforts of A. Baumgarten, J. Broeder, B. Beron, E. B. Hughes, and R. Parks, as well as those of the Linac and SPEAR staff at the Stanford Linear Accelerator Center. One of us (H.K.) received financial support from NATO, another (F.C.P.) from the Chaim Weizmann Foundation, and another (T.H.B.) from the A. P. Sloan Foundation. This work was supported in part by the Department of Energy under Contracts Nos. DE-AC03-76SF00515 (SLAC), EY-76-C02-3064 (Harvard), DE-AC03-81ER40050 (CIT), and DE-AC02-76ER03072 (Princeton); by the National Science Foundation under Contracts Nos. PHY81-07396 (HEPL), PHY79-16461 (Princeton), and PHY75-22980 (CIT).

---

[a]Permanent address: IntelliCorp, Mountain View, California 94040.

[b]Permanent address: Max-Planck Institute for Physics and Astrophysics, Munich, Federal Republic of Germany.

[c]Permanent address: SCIPP, University of California at Santa Cruz, Santa Cruz, California 95064.

[d]Permanent address: Enrico Fermi Institute, University of Chicago, Chicago, Illinois 60637.

[e]Permanent address: Theta Corporation, Mountain View, California 94041.

[f]Permanent address: Jet Propulsion Lab, Pasadena, California 91109.

[g]Permanent address: Institute of High Energy Physics, Academia Sinica, People's Republic of China.

[h]Permanent address: Hermann Distel Strasse 28, D-2050 Hamburg, Federal Republic of Germany.

[i]Permanent address: III Phys. Inst. der Techn. Hochschule, Aachen, Federal Republic of Germany.

[j]Permanent address: University of Cape Town, Physics Department, Cape Town, South Africa.

[k]Permanent address: Physics Department, University of Washington, Seattle, Washington 98195.

[l]Permanent address: Fermi National Accelerator Laboratory, Batavia, Illinois 60510.

[m]Permanent address: Computation Research Group, SLAC, Stanford, California 94305.

[n]Permanent address: CERN, EP-Division, Geneva, Switzerland.

[o]Permanent address: Universität Bonn, Bonn, Federal Republic of Germany.

[p]Permanent address: Universität Würzburg, Würzburg, Federal Republic of Germany.

[q]Permanent address: Schlumberger-Doll Research Center, Ridgefield, Connecticut 06877.

[r]Permanent address: VIDCO Inc., Cupertino, California 95014.

[s]Permanent address: Digital Applications International, Axtel House, 24 Warwick, London SW1, United Kingdom.

[1]For reviews of the charmonium model, see, T. Appelquist, R. M. Barnett, and K. Lane, Annu. Rev. Nucl. Part. Sci. **28**, 387 (1978); E. Eichten *et al.*, Phys. Rev. D **21**, 203 (1980); W. Buchmüller and S. H. Tye, *ibid.* **24**, 132 (1981); and more recently J. L. Rosner, in *Experimental Meson Spectroscopy—1983,* proceedings of the Seventh International Conference Brookhaven National Laboratory, 1983, edited by S. J. Lindenbaum (AIP Conf. Proc. No. 113) (AIP, New York, 1984); W. Buchmüller, lectures presented at the International School of Physics of Exotic Atoms, CERN Report No. TH-3938, Erice, 1984 (unpublished).

[2]V. A. Novikov *et al.*, Phys. Rep. **41C**, 1 (1978); M. A. Shifman, Pis'ma Zh. Eksp. Teor. Fiz. **30**, 547 (1979) [JETP Lett. **30**, 513 (1979)]; Z. Phys. C **4**, 345 (1980); M. A. Shifman and

M. I. Vysotsky, *ibid.* **10**, 131 (1980); A. Yu. Khodjamirian, Report No. EFI-427-34-80, 1980 (unpublished); A. Yu. Khodjamirian, Phys. Lett. **90B**, 460 (1980); Yad. Fiz. **39**, 970 (1984) [Sov. J. Nucl. Phys. **39**, 614 (1984)].

[3]R. Barbieri, R. Gatto, and E. Remiddi, Phys. Lett. **61B**, 465 (1976); R. Barbieri, M. Caffo, R. Gatto, and E. Remiddi, *ibid.* **95B**, 93 (1980); R. Barbieri, R. Gatto, E. Remiddi, *ibid.* **106B**, 497 (1981); E. Eichten and F. Feinberg, Phys. Rev. D **23**, 2724 (1981); J. Arafume and M. Fukugita, Phys. Lett. **102B**, 437 (1981); R. McClary and N. Byers, Phys. Rev. D **28**, 1692 (1983).

[4]J. S. Whitaker *et al.*, Phys. Rev. Lett. **37**, 1596 (1976).

[5]C. J. Biddick *et al.* Phys. Rev. Lett. **38**, 1324 (1977). We give their results: $B(\psi'\to\gamma\chi_{2,1,0})=(0.70\pm0.020)$, (0.071 ± 0.019), and (0.072 ± 0.023), respectively.

[6]The spins of the $\chi_{2,1}$ states have been measured by the Crystal Ball experiment in the exclusive reaction $\psi'\to\gamma\gamma l^+l^-$, see Ref. 13.

[7]C. Baglin *et al.*, in *Hadron Spectroscopy—1985;* proceedings of the International Conference, College Park, Maryland, 1985, edited by S. Oneda (AIP Conf. Proc. No. 132) (AIP, New York, 1985).

[8]R. Partridge *et al.*, Phys. Rev. Lett. **45**, 1150 (1980).

[9]T. M. Himel *et al.*, Phys. Rev. Lett. **45**, 1146 (1980).

[10]R. M. Baltrusaitis *et al.*, Phys. Rev. D **33**, 629 (1986).

[11]C. Edwards *et al.*, Phys. Rev. Lett. **48**, 70 (1982).

[12]F. C. Porter *et al.*, in *Proceedings of the Seventeenth Recontre de Moriond,* Les Arcs, France, 1982, edited by J. Tran Thanh Van (Editions Frontières, Gif-sur-Yvette, 1982), p. 27.

[13]M. Oreglia, Ph.D. thesis, Stanford University, SLAC Report No. 236, 1980.

[14]M. Oreglia *et al.*, Phys. Rev. D **25**, 2259 (1982). We give the results for the product branching ratios: $B(\psi'\to\gamma\chi_J)B(\chi_J\to\gamma J/\psi)=(0.059\pm0.017)\%$, $(2.38\pm0.33)\%$, and $(1.26\pm0.18)\%$ for $J=0,1,2$ respectively, after removing the normalization error common to the inclusive gamma measurement.

[15]J. E. Gaiser, Stanford University Report No. SLAC-255, 1982.

[16]R. L. Ford and W. R. Nelson, Stanford University Report No. SLAC-210, 1978 (unpublished).

[17]This procedure assumes that the multihadronic decays of the χ are similar to those of the J/ψ. Since the masses of χ and J/ψ are close the multiplicity of decay products is also expected to be similar.

[18]See, for example, Eichten *et al.*, Ref. 1.

[19]The parent state's natural linewidths are sufficiently small (0.063 ± 0.009 MeV for the J/ψ and 0.215 ± 0.040 MeV for the ψ') that they can be neglected.

[20]The width of the χ_1 state is expected to be very narrow. See for example Appelquist *et al.*, Ref. 1.

[21]R. A. Lee, Stanford University Report No. SLAC-282, 1985.

[22]We believe that the two independent measurements of the χ_0 natural linewidth are equally valid. Hence we give their weighted average as our best estimate of the width. For this calculation a normal distribution around the central value of the inclusive measurement range is adequate, and we add statistical and systematic errors of the exclusive measurement linearly. To be conservative, we estimate from the difference of the two measurements a possible contribution from an additional and unknown systematic error source of ±4.2 MeV. The final error quoted covers both measurements.

[23]Eichten and Feinberg, (Ref. 3).

[24]M. G. Olsson *et al.*, Phys. Rev. D **25**, 81 (1985); Barbieri *et al.* (Ref. 3).

[25]For example, McClary and Byers (Ref. 3).

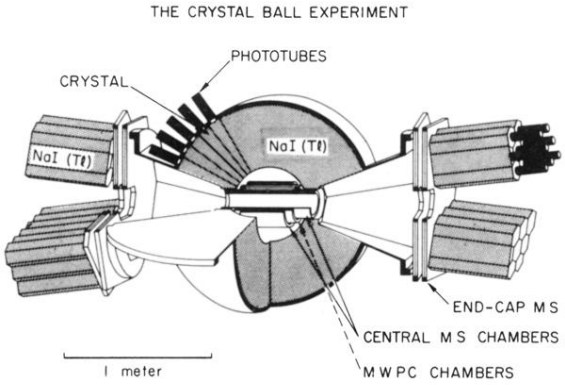

FIG. 1. Schematic view of the Crystal Ball detector.